



***Plasmodium falciparum* SSB Tetramer Wraps Single-Stranded DNA with Similar Topology but Opposite Polarity to *E. coli* SSB**

Edwin Antony¹, Elizabeth A. Weiland¹, Sergey Korolev^{2*} and Timothy M. Lohman^{1*}

¹Department of Biochemistry and Molecular Biophysics, Washington University School of Medicine, 660 South Euclid Avenue, Box 8231, St. Louis, MO 63110-1093, USA

²Edward A. Doisy Department of Biochemistry and Molecular Biology, Saint Louis University School of Medicine, 1100 South Grand Boulevard, St. Louis, MO 63104, USA

Received 11 January 2012;
received in revised form
16 March 2012;
accepted 6 April 2012
Available online
27 April 2012

**Edited by S.
Kowalczykowski**

Keywords:

DNA repair;
recombination;
replication;
structure;
Plasmodium and malaria

Single-stranded DNA binding (SSB) proteins play central roles in genome maintenance in all organisms. *Plasmodium falciparum*, the causative agent of malaria, encodes an SSB protein that localizes to the apicoplast and likely functions in the replication and maintenance of its genome. *P. falciparum* SSB (Pf-SSB) shares a high degree of sequence homology with bacterial SSB proteins but differs in the composition of its C-terminus, which interacts with more than a dozen other proteins in *Escherichia coli* SSB (Ec-SSB). Using sedimentation methods, we show that Pf-SSB forms a stable homo-tetramer alone and when bound to single-stranded DNA (ssDNA). We also present a crystal structure at 2.1 Å resolution of the Pf-SSB tetramer bound to two (dT)₃₅ molecules. The Pf-SSB tetramer is structurally similar to the Ec-SSB tetramer, and ssDNA wraps completely around the tetramer with a “baseball seam” topology that is similar to Ec-SSB in its “65 binding mode”. However, the polarity of the ssDNA wrapping around Pf-SSB is opposite to that observed for Ec-SSB. The interactions between the bases in the DNA and the amino acid side chains also differ from those observed in the Ec-SSB–DNA structure, suggesting that other differences may exist in the DNA binding properties of these structurally similar proteins.

© 2012 Elsevier Ltd. All rights reserved.

Introduction

Plasmodium falciparum is a eukaryotic parasite and the causative agent for over 250 million cases of

malaria that result in 5 million deaths annually.¹ It contains a unique non-photosynthetic plastid-like organelle called the apicoplast, which is involved in a variety of biosynthetic pathways of the parasite. A single apicoplast is present in each cell and functions in isoprenoid, fatty acid and heme synthesis/metabolism and is critical to parasite survival and pathogenesis, making it a logical target for antimalarial drugs. The ~ 35-kb apicoplast genome contains 68 open reading frames that encode a variety of ribosomal proteins, tRNAs, RNA polymerase, chaperones and other proteins of unknown function.² However, proteins involved in DNA metabolism are encoded by the nuclear DNA and targeted for transport to the apicoplast by an

*Corresponding authors. E-mail addresses: korolevs@slu.edu; lohman@biochem.wustl.edu.

Abbreviations used: TCEP, tris(2-carboxyethyl) phosphine; 2-ME, 2-mercaptoethanol; ALS, apicoplast localization signal; SSB, single-stranded DNA binding; ssDNA, single-stranded DNA; Pf-SSB, *P. falciparum* SSB; Ec-SSB, *Escherichia coli* SSB; PDB, Protein Data Bank; EDTA, ethylenediaminetetraacetic acid; PEI, polyethylenimine; PEG, polyethylene glycol.

apicoplast localization signal (ALS), which is cleaved upon delivery to the apicoplast.³ The single-stranded DNA binding (SSB) protein from *P. falciparum* [*P. falciparum* SSB (*Pf*-SSB)] is encoded in the nucleus and transported to the apicoplast where it likely functions in the replication and maintenance of the apicoplast genome.⁴

SSB proteins are present in nearly all organisms and bind to single-stranded DNA (ssDNA) intermediates produced transiently during replication, repair and recombination. *Escherichia coli* SSB (*Ec*-SSB) is a well-characterized prototype of bacterial SSB proteins⁵ and shares high sequence homology with *Pf*-SSB (39% identity and 66% homology).⁴ *Ec*-SSB functions as a homo-tetramer with each subunit consisting of two domains, an N-terminal OB-fold containing the ssDNA binding site and an unstructured C-terminal tail.^{5–7} *Ec*-SSB also interacts with more than a dozen other proteins involved in DNA metabolism.⁸ These interactions are primarily mediated through a conserved stretch of 8–10 amino acids located at the end of its unstructured C-termini.⁸

In the case of *Ec*-SSB, it has been shown that, at moderate to high salt concentrations, an ssDNA ~65 nucleotides long can fully wrap around the tetrameric DNA binding core to form the so-called (SSB)₆₅ binding mode.^{9–11} However, due to its four potential DNA binding sites, *Ec*-SSB can also bind to long ssDNA in a number of different binding modes that differ by the number of subunits (OB-folds) within the tetramer that contact the DNA.^{10,12,13} In the (SSB)₆₅ mode, ssDNA interacts with all four subunits and displays little tendency to form cooperative clusters along ssDNA.^{14,15} The low cooperative,

fully wrapped (SSB)₆₅ binding mode has been proposed to facilitate RecA-mediated DNA strand exchange during homologous recombination.^{16–18} In fact, *Ec*-SSB, while bound in its (SSB)₆₅ mode, is able to diffuse along ssDNA and transiently melt DNA hairpins, thus facilitating RecA filament formation along ssDNA.¹⁸ Here, we present a structural study of the *Pf*-SSB protein and its complexes with ssDNA including a crystal structure of a *Pf*-SSB tetramer in complex with ssDNA in a fully wrapped binding mode allowing a detailed comparison of its structure with *Ec*-SSB.

Results

Pf-SSB forms a stable homo-tetramer in solution

SSB proteins can exist in a variety of oligomeric states including monomers (e.g., T4 phage gp32),¹⁹ dimers (e.g., *Deinococcus radiodurans* SSB),²⁰ trimers (e.g., eukaryotic RPA),²¹ tetramers (most bacterial SSBs)⁸ and pentamers (e.g., *D. radiodurans* DdrB).²² Based on dynamic light scattering and sucrose density gradient analysis, a histidine-tagged version of recombinant *Pf*-SSB appears to behave as a homo-tetramer in solution.⁴ Here, we examined the assembly state of an untagged version of *Pf*-SSB using analytical sedimentation methods. In sedimentation velocity experiments of *Pf*-SSB in the absence of reducing agents (3 μ M *Pf*-SSB, buffer H^{0.2} at 25 °C), we observe three or more distinct species with average sedimentation coefficients of 5.3 ± 0.2 , 8.1 ± 0.4 and 11.2 ± 0.7 S with predicted molecular

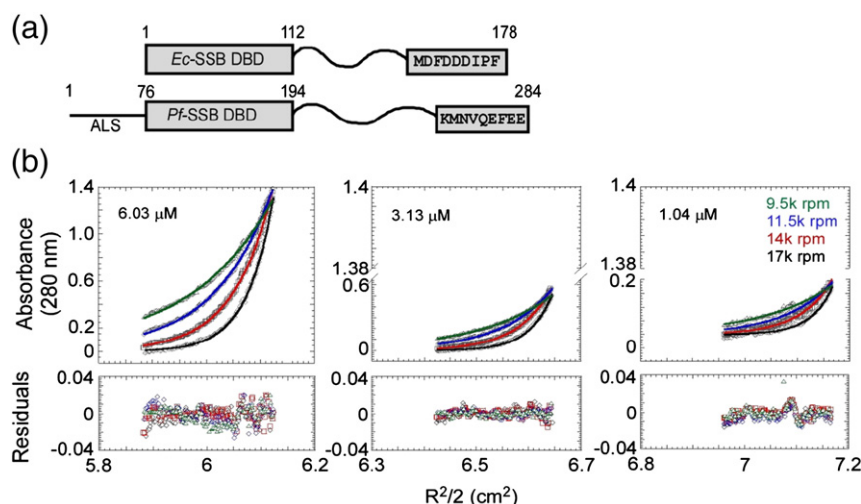


Fig. 1. *Pf*-SSB is a stable homo-tetramer in solution. (a) Domain architecture of *Pf*-SSB and *Ec*-SSB proteins. (b) Sedimentation equilibrium experiments indicate that *Pf*-SSB is a stable homo-tetramer in solution. Experiments were performed at three different protein concentrations as indicated in the plot and at four rotor speeds (9500, green; 11,500, blue; 14,000, red; 17,000, black). The smooth lines depict the fits to a single-species model, and the appropriate residuals are also shown.

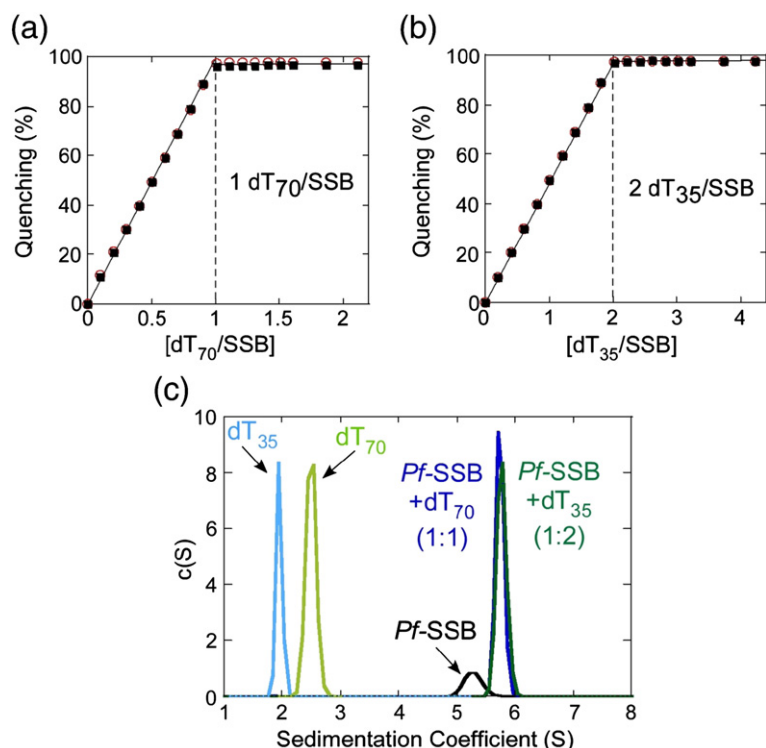


Fig. 2. *Pf*-SSB binds stoichiometrically to DNA. Fluorescence experiments show the quenching of tryptophan fluorescence upon binding to (dT)₇₀ (a) or (dT)₃₅ (b) DNA oligonucleotides. The broken lines show the stoichiometric binding of either one molecule (dT)₇₀ or two molecules (dT)₃₅ per *Pf*-SSB tetramer. (○) and (■) represent experiments performed at either 0.1 or 0.3 μM *Pf*-SSB in the reaction, respectively. (c) Continuous sedimentation coefficient distribution *c*(*s*) analysis of *Pf*-SSB in the presence or absence of ssDNA. *Pf*-SSB sediments as a single tetrameric species in the absence of DNA (black) and is capable of stoichiometrically binding two (dT)₃₅ molecules (when mixed in a 1:2 ratio; dark-green trace) or one (dT)₇₀ molecule (mixed in a 1:1 ratio; dark-blue trace). Sedimentation profiles of (dT)₃₅ (light green) or (dT)₇₀ (light blue) in the absence of protein are also depicted.

masses corresponding to tetramer (92.7 kDa), octamer (176 kDa) and dodecamer (280 kDa; Fig. S1a). Since *Pf*-SSB has a native cysteine at position 93, we tested whether disulfide bond formation influences the oligomerization by repeating the experiments in the presence of reducing agents [either 5 mM 2-mercaptoethanol (2-ME) or 1 mM tris(2-carboxyethyl)phosphine (TCEP)]. In the presence of reducing agents in buffer H^{0.2}, *Pf*-SSB displays a single symmetrical peak in a continuous sedimentation [*c*(*s*)] analysis^{23,24} consistent with a single species (Fig. S1b), with a weight average sedimentation coefficient of 5.28 ± 0.16 S, corresponding to a predicted molecular mass of 92.5 kDa and a frictional coefficient ratio (f/f_0) of 1.39 ± 0.03 . This is close to the expected molecular mass for a *Pf*-SSB homo-tetramer (98,296 Da) as calculated from its amino acid composition.

We also used sedimentation equilibrium to obtain a rigorous molecular weight estimate of *Pf*-SSB. The results of experiments performed at three *Pf*-SSB concentrations [1.04, 3.13 and 6.03 μM (tetramer)] and four speeds (9500, 11,500, 14,000 and 17,000 rpm) are shown in Fig. 1b. Global NLLS (nonlinear least-squares) analysis of these data gave results consistent with a single ideal species [Eq (1) and Materials and Methods] with an average molecular mass of $M_r = 98,824 \pm 221$ Da. This value agrees well with the predicted molecular mass of 98,296 Da for a *Pf*-SSB homo-tetramer. Hence, *Pf*-SSB is a stable homo-tetramer over a concentration range from 0.5 to 6 μM (tetramer).

Pf-SSB binds tightly to ssDNA

Ec-SSB contains four Trp residues per monomer (three in the DNA binding core), and ssDNA binding can be monitored by the quenching of its intrinsic Trp fluorescence (~90% at saturation).^{10,25} The *Ec*-SSB tetramer binds to DNA with very high affinity, and 65 nucleotides of poly(dT) are required to fully wrap around the tetramer.¹⁰ As such, an *Ec*-SSB tetramer can bind either one molecule of (dT)₇₀ or two molecules of (dT)₃₅.²⁶ *Pf*-SSB contains three Trp residues per monomer in the same conserved positions within the DNA binding core, and its Trp fluorescence is also quenched upon binding ssDNA (see below). For *Pf*-SSB, we have measured an occluded site size of 62 ± 2 nucleotides per *Pf*-SSB tetramer on poly(dT) at high [NaCl] (>0.2 M) (Antony *et al.*, accompanying paper). In preparation for attempts at crystallizing *Pf*-SSB with ssDNA, we examined the binding of *Pf*-SSB to both (dT)₇₀ and (dT)₃₅ by monitoring the accompanying change in *Pf*-SSB tryptophan fluorescence (buffer H^{0.2} at 25 °C) as shown in Fig. 2a and b. These titrations show that, under these conditions, *Pf*-SSB binds very tightly to both (dT)₇₀ and (dT)₃₅ such that we can only estimate a binding stoichiometry but not an affinity. The *Pf*-SSB tetramer can bind either one molecule of (dT)₇₀ (Fig. 2a) or two molecules of (dT)₃₅ (Fig. 2b) per tetramer, and in both cases, almost complete quenching (96–98%) of the Trp fluorescence is observed. By comparison with the Trp fluorescence quenching observed for (dT)₇₀ and (dT)₃₅ binding of

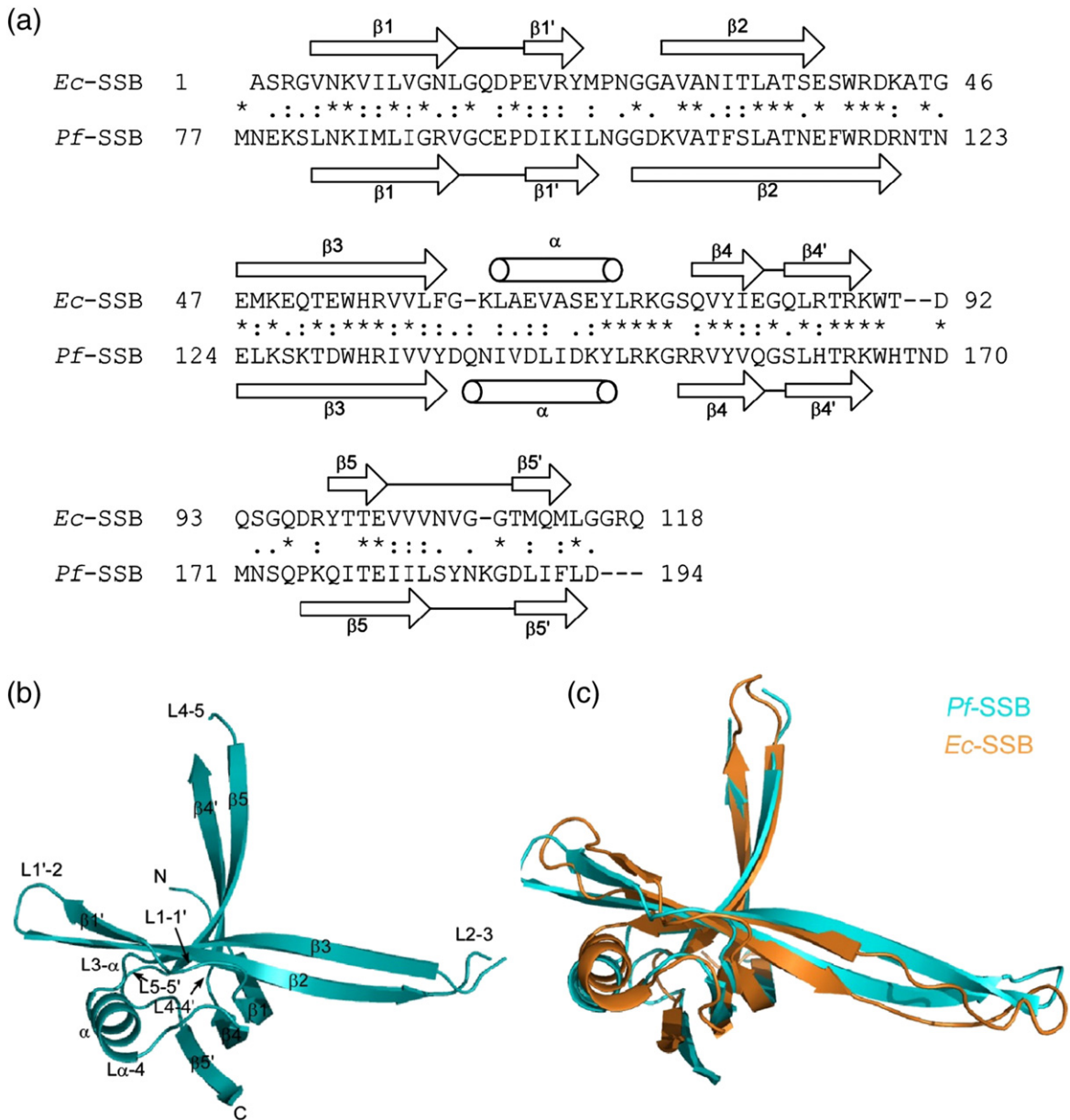


Fig. 3. Crystal structure of *Pf*-SSB. (a) Sequence alignment of *Pf*-SSB and *Ec*-SSB and a schematic representation of their secondary structure. Strictly conserved residues are marked by an asterisk (*). (b) Architecture of a single monomer in *Pf*-SSB. (c) Overlay of a single monomer from *Pf*-SSB (cyan) and *Ec*-SSB (orange) highlights the similarity in protein structure between the two proteins.

Ec-SSB, these results suggest that one molecule of (dT)₇₀ or two molecules of (dT)₃₅ can bind to *Pf*-SSB, both resulting in complete wrapping of DNA around the *Pf*-SSB tetramer. One interesting difference between *Pf*-SSB and *Ec*-SSB is the lack of apparent negative cooperativity in the binding of the second molecule of (dT)₃₅ to the *Pf*-SSB tetramer (see Antony *et al.*, accompanying paper), whereas *Ec*-SSB tetramer shows clear negative cooperativity.^{26–28}

We also examined *Pf*-SSB and its ssDNA complexes using sedimentation velocity. *Pf*-SSB tetramers, when

bound to either two molecules of (dT)₃₅ or one molecule of (dT)₇₀, displayed *c(s)* profiles²³ with single symmetrical peaks with $s_{20,w} = 5.73 \pm 0.07$ S and 5.76 ± 0.09 S, respectively (Fig. 2c), corresponding to predicted molecular masses of 133.6 and 133.58 kDa, respectively. The f/f_0 values calculated from these experiments are 1.39 ± 0.02 , 1.63 ± 0.02 and 1.63 ± 0.03 for *Pf*-SSB alone and the *Pf*-SSB–(dT)₃₅ and *Pf*-SSB–(dT)₇₀ complexes, respectively. Therefore, *Pf*-SSB bound to either one (dT)₇₀ or two (dT)₃₅ molecules displays similar hydrodynamic properties.

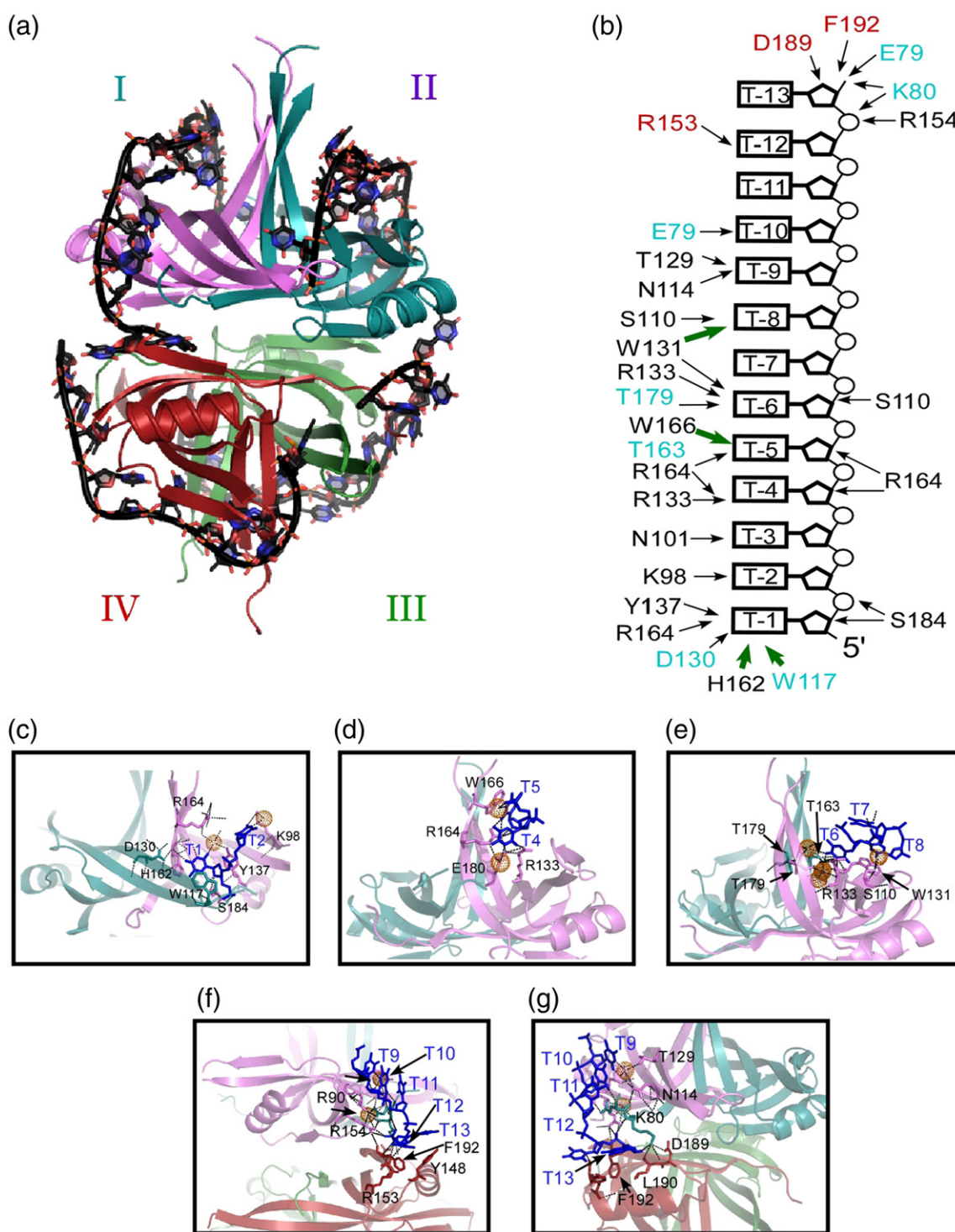


Fig. 4. A homo-tetramer of Pf-SSB binds to ssDNA. (a) The subunits of the Pf-SSB tetramer are colored cyan, violet, green and red with the two bound (dT)₃₅ molecules shown as sticks (black). (b) Schematic of DNA residues 1–13 that are observed in the monomer bound to the purple subunit and residues in Pf-SSB that interact with the DNA are shown. The residues colored red and blue are from the red and blue subunits, respectively, and all other residues are from the violet subunit. The bold-green arrows denote stacking interactions between the bases and the aromatic amino acid side chains. Details of the interactions between DNA bound to the violet subunit in Pf-SSB and the amino acid side chains are depicted with respect to nucleotides T1–T3 (c), T4–T5 (d), T6 and T8 (e) and T9 and T13: front view (f) and back view (g and f). The orange spheres denote density for either water or probable ion molecules in the structure that mediate specific interactions between the protein and the DNA.

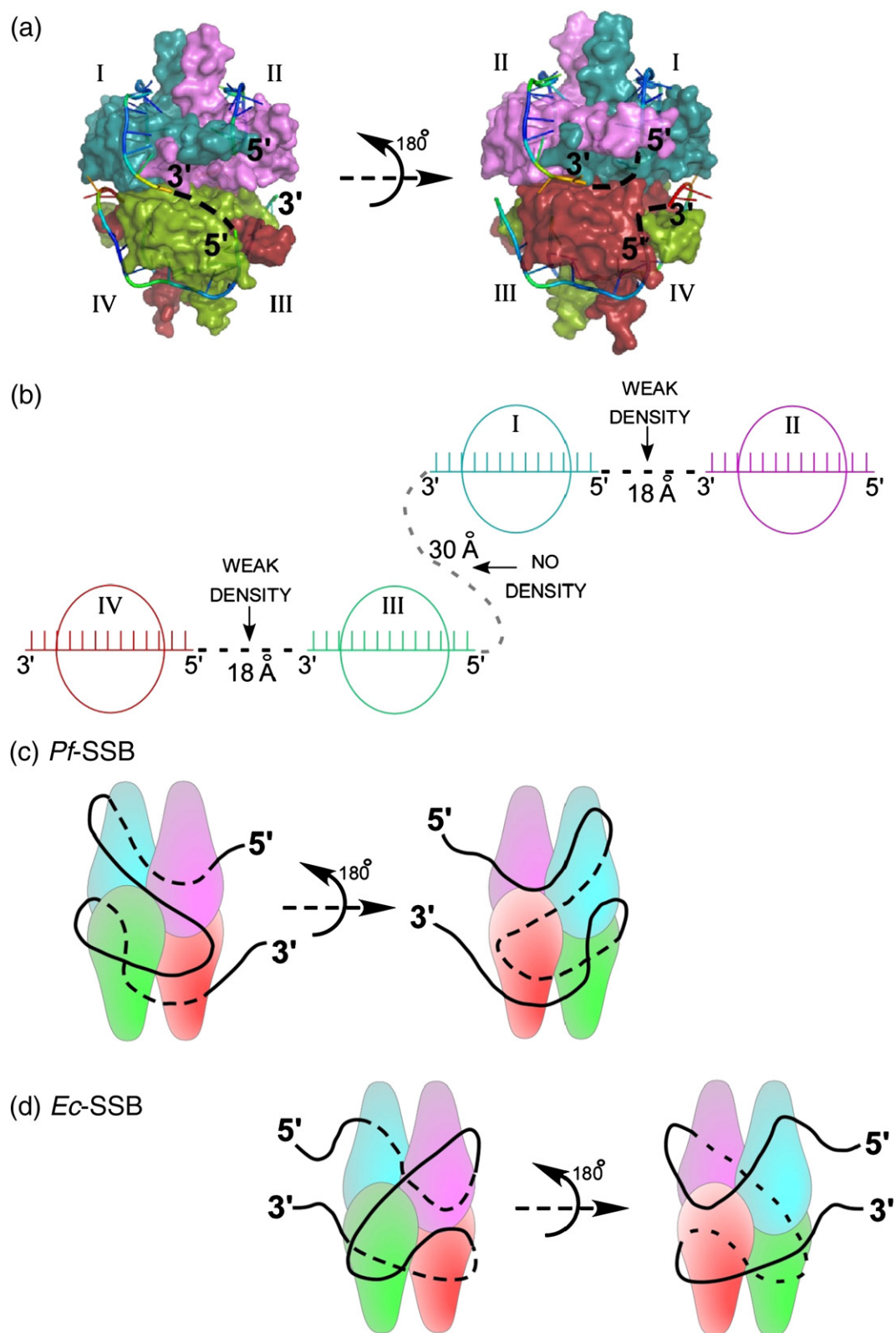


Fig. 5 (legend on next page)

Crystal structure of *Pf*-SSB is similar to that of *Ec*-SSB

We have solved a crystal structure at 2.1 Å resolution of *Pf*-SSB in complex with two molecules of (dT)₃₅. The *Pf*-SSB used in the crystallization contained amino acid residues 77–284. Residues 1–76 are part of the ALS (Fig. 1a) and are cleaved upon arrival at the apicoplast,^{29,30} hence, we did not include these in the recombinant protein that we expressed and purified. We observed two crystal forms with either a monomer or a tetramer in the asymmetric unit (Fig. S2). In both cases, we only observe electron density for the amino acids that form the DNA binding core (residues 77–194). Upon analysis of the crystals using SDS-PAGE, the protein component that had crystallized migrated faster than the full-length starting protein, suggesting that the C-terminal part of the protein was at least partially cleaved (Fig. S2c). Since we observe excellent density for residues 77–194, the cleavage must occur after residue 194; however, we have not determined the precise site of cleavage. Similar proteolytic cleavage has been observed during crystallization of the *Ec*-SSB protein.^{11,31–33} Since the structural details of both *Pf*-SSB–(dT)₃₅ crystal forms are similar, we discuss only the structure derived from the crystal form showing the tetramer in the asymmetric unit.

Each subunit contains an oligosaccharide/oligonucleotide-fold (OB-fold) found in many SSB proteins³⁴ (Fig. 3a) and is composed of five β-strands (β1–β5) and one α-helix (α) connected by short linkers (L1–1', L1'–2, L2–3, L3–α, Lα–4, L4–4', L4–5 and L5–5'; Fig. 3b). All four subunits in the tetramer have similar conformations with RMSD values ranging from 0.12 to 0.26 Å for 90–95 C^α atoms. The overall structure resembles the *Ec*-SSB tetramer, and 77 C^α atoms of *Pf*-SSB and *Ec*-SSB monomers align with an RMSD of 0.8 Å (Fig. 3c). Alignment was performed using PyMOL with the default cutoff level of 2 Å. Noticeable differences in the *Pf*-SSB structure are the more ordered 4–5 and 2–3 β-sheets and the disordered tips of the 4–5 loops (Fig. 3c). *Pf*-SSB and *Ec*-SSB tetramers align with an RMSD of 8.6 Å for 306 C^α atoms reflecting minor differences in the mutual orientation of individual subunits (Fig. S3). Both proteins show a high degree of structural similarity in the overall architecture of

the DNA binding domains and the organization of the homo-tetramer.

ssDNA wraps around the *Pf*-SSB tetramer interacting with all four subunits

Since *Pf*-SSB binds tightly to either one molecule of (dT)₇₀ or two molecules of (dT)₃₅ (Fig. 2), we formed and obtained crystals of each of these complexes. Crystals of *Pf*-SSB with two bound (dT)₃₅ molecules diffracted to 2.1 Å, although interpretable density is observed for only 25 nucleotides per (dT)₃₅ molecule (Fig. 4a), and a majority of the modeled DNA is well ordered (Fig. S4). We have numbered the nucleotides T₁–T₁₄ and T₁₈–T₂₈ (Fig. 4b) [since the DNA is an oligo(dT), T-1 may not be the actual 5' end of the DNA molecule]. We assumed that the gap between the two ordered ssDNA segments was missing three nucleotides based on the distance between the ends of the ssDNA segments and the presence of weak electron density potentially corresponding to the missing nucleotides. Although we observe some density consistent with two or three bases corresponding to residues T₁₅–T₁₇, the density cannot be fit to a single conformation, suggesting that this region is disordered. We also obtained small crystals that diffracted to 3.8 Å for *Pf*-SSB bound to a molecule of (dT)₇₀ but were unable to obtain a structure of this complex due to the poor quality of the crystals. These crystals were of the same space group as the *Pf*-SSB–(dT)₃₅ complex, suggesting that (dT)₇₀ is bound in a conformation similar to that of the two (dT)₃₅ molecules.

Protein–DNA contacts

In the *Pf*-SSB–(dT)₃₅ structure, the residues that contact the DNA are identical in all four subunits (Fig. 4). This differs from the asymmetric contacts observed in the *Ec*-SSB–(dC)₃₅ structure.¹¹ A schematic of the specific contacts between amino acids in one monomer and the DNA is shown in Fig. 4b. Residues from three different subunits contact each half of the (dT)₃₅ molecule. We also observe density for several water molecules and/or ions; since it is difficult to distinguish between electron density for water molecules *versus* ions at 2.1 Å resolution, all solvent molecules in the structure are modeled and discussed as waters. The first nucleotide in the DNA

Fig. 5. Models for DNA wrapping around *Pf*-SSB. (a) A space-filled version of the *Pf*-SSB structure with the bound DNA colored according to its B-factor. The predicted path of a (dT)₇₀ DNA molecule is shown by broken lines traversing across the tetramer, and the path of the missing DNA residues in each (dT)₃₅ molecule is also denoted by broken lines. (b) A schematic depicting the polarity of each (dT)₃₅ molecule bound to the four subunits in the *Pf*-SSB tetramer. The black broken lines represent regions of the DNA for which we observe weak density, and the gray broken line connecting the two (dT)₃₅ molecules is a predicted path for wrapping of a (dT)₇₀ molecule. (c) Cartoon representation showing the front and back views of DNA wrapping around the *Pf*-SSB tetramer. (d) The path of DNA wrapping around the *Ec*-SSB tetramer.¹¹

for which we observe density, denoted T-1, contacts both the 2–3 loop of one subunit and the 1–2 loop of the adjacent subunit. R164 and Y137 contact T-1 through a water molecule, and H162 and W117 (subunit I) form stacking interactions with T-1. D130 contacts both T-1 and H162 through water molecules. S184 contacts both the backbone phosphate and the sugar moiety (Fig. 4c). T-2 makes a contact with K98 through another water molecule, and T-3 contacts N101 (Fig. 4d). R164 also contacts both T-4 and T-5 bases and their respective sugars along with its aforementioned contact with T-1. R133 contacts T-4 and forms a network with E180, R164 and the DNA. Two threonines (T163 and T179) from subunit I coordinate the T-5 and T-6 bases through two waters, and the backbone of T-6 makes a contact with S110 (Fig. 4e). W166 forms a stacking interaction with T-5, and this conserved residue assists in bending of the DNA around the individual monomer. W131 is homologous to the functionally critical W54 in *Ec*-SSB^{35–38} and makes a base-stacking interaction with T-8. W131 also makes a polar contact with T-6 at which point the DNA bends around the 1–2 loop and funnels toward the other half of the subunit (Fig. 4e).

S110 contacts T-8, N114 and T129 contacts T-9 and along with E79 from subunit I interacts with the bend in the DNA formed by residues T-8 through T-10. T-12 and T-13, the last two residues for which we observe electron density, interact with the N-terminus of subunit I (E79 and K80) and the C-terminus of the subunit IV (R153, D189 and F192). Together with R154, they form a series of well-networked connections that may control the entry of the DNA into the next subunit (Fig. 4f and g).

Topology of DNA wrapping around the *Pf*-SSB tetramer

Although we were unable to solve a structure of the *Pf*-SSB tetramer bound to (dT)₇₀, we were able to use the structure of the complex with two (dT)₃₅ molecules bound to identify the most likely path of the ssDNA in a fully wrapped complex (Fig. 5a). There are four DNA fragments in our structure that show clear electron density for 13–14 nucleotides bound per subunit (Fig. 5b). We observe weak density for two to four nucleotides that lie between the DNA fragments bound to subunits I and II and between subunits III and IV (Fig. 5b), and the spacing in these gaps is small (<18 Å). Hence, we assume that these short gaps reflect disordered regions of the two (dT)₃₅ molecules (Fig. 5b). We next need to decide the path that a (dT)₇₀ molecule would follow in a fully wrapped structure. The 3' end of the DNA bound to subunit I and the 5' end of the DNA bound to subunit III would likely be connected if part of a continuous (dT)₇₀ molecule since the ends are unobstructed in the structure and the distance between them is ~30 Å (Fig. 5a and b). Based on this, a model for how DNA might wrap completely around the *Pf*-SSB tetramer is shown in Fig. 5c. This proposed path of the ssDNA follows a topology similar to the seams on a baseball as previously found for the *Ec*-SSB–(dC)₃₅ structure¹¹ (Fig. 5d), although the backbone polarity is opposite to that observed in the *Ec*-SSB structure (see below for discussion of polarity).

Based on this crystal structure, we cannot completely exclude the alternate pathway for DNA wrapping around the tetramer, where the 5' end of

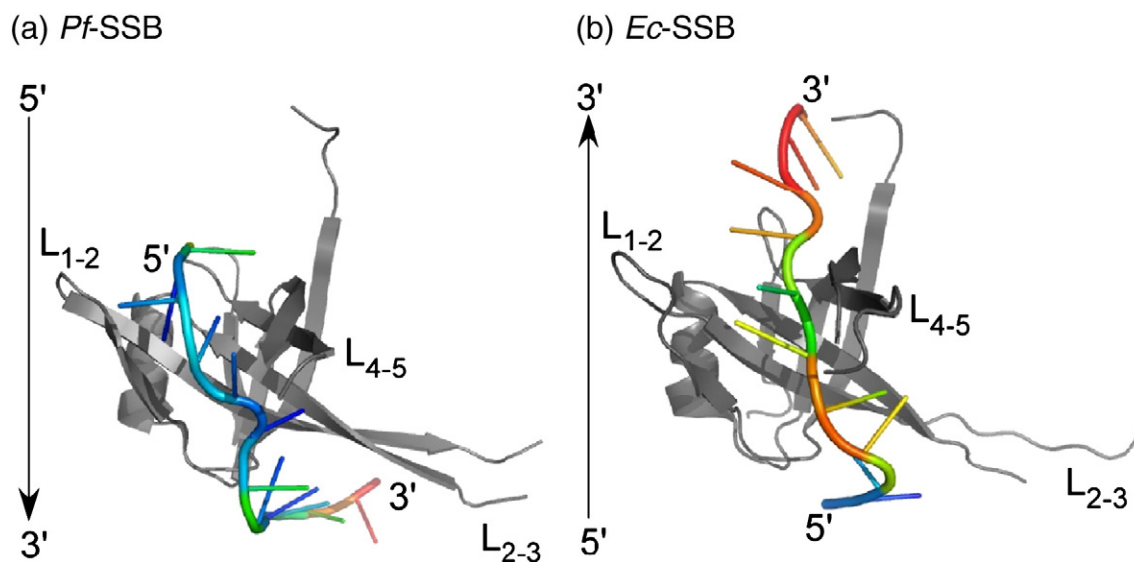


Fig. 6. ssDNA wraps around *Pf*-SSB with polarity opposite to *Ec*-SSB. Polarity of the ssDNA bound across a monomer in (a) *Pf*-SSB and (b) *Ec*-SSB. The DNA is bound with a 5'-to-3' polarity from top to bottom in the *Pf*-SSB structure and with opposite polarity in the *Ec*-SSB structure.

the DNA bound to subunit II connects with the 3' end of the DNA bound to subunit III (Fig. 5a and b). If this were to be the case, then a “baseball seam”-like topology for wrapping would not hold true. However, the 5' end of the DNA bound to subunit II, which is buried within the protein due to the closure of the L_{2-3} and L_{1-2} loops, must become available and would require significant movement of both these loops away from each other in order to accommodate this alternate path.

We observe ~ 26 nucleotides bound to each half of the tetramer, and the ~ 30 -Å gap between the 5' and 3' ends of the DNA can be filled with ~ 5 nucleotides (Fig. 5b). The shorter ~ 18 -Å gap would accommodate ~ 3 nucleotides (Fig. 5b); hence, ~ 61 – 64 nucleotides of ssDNA would be required to completely wrap around the entire tetramer. Indeed, this estimate is consistent with the occluded site size of 62 ± 2 nucleotides for the *Pf*-SSB tetramer on poly(dT) DNA measured under high salt conditions (buffer $H^{0.2}$) (Antony *et al.*, accompanying paper).

We observe excellent density for the DNA in our structure, and the 2.1-Å resolution is sufficient to determine the backbone polarity of the DNA bound to *Pf*-SSB. Interestingly, the backbone polarity of the (dT)₃₅ molecules within the *Pf*-SSB complex (Fig. 6a) is opposite to that observed in the *Ec*-SSB–(dC)₃₅ structure (Fig. 6b). In the *Pf*-SSB structure, the 5' end of the DNA binds to the L_{1-2} loop and is extended through contacts with the L_{4-5} loop toward loop L_{2-3} (Fig. 6a). In the DNA-bound structures of *Mycobacterium smegmatis* SSB [Protein Data Bank (PDB) code: 3A5U] and *Helicobacter pylori* SSB,³⁹ the polarity of the bound DNA is the same as observed in the *Pf*-SSB structure.

Discussion

We describe a crystal structure of the *Pf*-SSB tetramer bound to ssDNA at 2.1 Å resolution. All four subunits interact with the ssDNA, and the topology of the DNA path resembles the “seams of a baseball” as observed for *Ec*-SSB in its fully wrapped (SSB)₆₅ DNA binding mode (Fig. S5).¹¹ Although crystal structures of SSB proteins from multiple organisms have been reported in their apo-form,^{20,40–45} only three SSB–DNA complex structures have been reported.^{11,39} Of these, only the crystal structure of the *Ec*-SSB DNA complex was crystallized with the entire tetramer in the asymmetric unit, and the density for 26–28 of the 35 nucleotides in each of the two bound (dC)₃₅ DNA molecules was observed, thereby providing sufficient information to determine the topology of the wrapped ssDNA.¹¹ In the *Pf*-SSB–(dT)₃₅ structure reported here, we also observe electron density for the entire tetramer and for 25–26 nucleotides of each

of the two molecules of (dT)₃₅ bound to the protein (Fig. S4). We find that ssDNA wraps around the *Pf*-SSB tetramer with a topology similar to that of *Ec*-SSB but with opposite polarity. There are three notable differences between the *Pf*-SSB and *Ec*-SSB structures: (a) protein–DNA contacts, (b) the symmetry of the DNA contacts in the four subunits and (c) the protein–protein contacts between adjacent tetramers. If and how these factors contribute to the observed difference in polarity of DNA wrapping, DNA binding activity or DNA binding modes remains to be determined (see Antony *et al.*, accompanying paper).

In the *Pf*-SSB structure, an extensive network of interactions between the amino acid side chains and the bases of the DNA is apparent (Fig. 4). These interactions can be divided into stacking interactions between the aromatic protein side chains and the nucleotides, ionic and polar contacts and contacts between the protein and the phosphate backbone of the DNA. In both *Ec*-SSB and *Pf*-SSB structures, significant interactions occur through stacking interactions between the bases in the DNA and three tryptophan residues per subunit (W117, W131 and W166 in *Pf*-SSB). The aromatic side chains of these tryptophans stack against the pyrimidine bases T1, T8 and T5, respectively (Fig. 4). These residues are also conserved in *Ec*-SSB (W40, W54 and W88), but only two of the three Trp residues (W54 and W88) base stack with similar orientations in all four subunits. W40 is located on the 2–3 loop and adopts multiple conformations in the four subunits of *Ec*-SSB due to the flexible nature of the loop. The homologous W117 residue in *Pf*-SSB is not positioned on the 2–3 loop but is located on the structured β -sheet 2 and adopts the same conformation in all four subunits. In *Pf*-SSB, we observe 98% quenching of the Trp fluorescence upon saturation with two molecules of (dT)₃₅ or one molecule of (dT)₇₀. This is consistent with the observation that all three of the Trp residues in *Pf*-SSB form stacking interactions with the DNA bases and that the fluorescence of each is essentially fully quenched. *Pf*-SSB also uses a unique set of charged residues to mediate electrostatic interactions with the DNA phosphates. R90, K128, R153 and R154 form electrostatic interactions with the DNA, but these residues are not conserved in *Ec*-SSB (Fig. 3). In *Ec*-SSB, histidine 55 contributes to the stability of the tetramer in that a H55Y mutation (*ssb-1*) destabilizes the tetramer in favor of monomers.^{46–48} This *ssb-1* mutation results in a temperature-sensitive phenotype *in vivo*.^{49,50} The homologous residue, H132 in *Pf*-SSB, is also located at the same position and makes *inter*-subunit contacts with N83 and L160 (N6 and L83 are the homologous residues in *Ec*-SSB).

Another difference between the *Ec*-SSB and *Pf*-SSB structures is that the protein–DNA contacts are

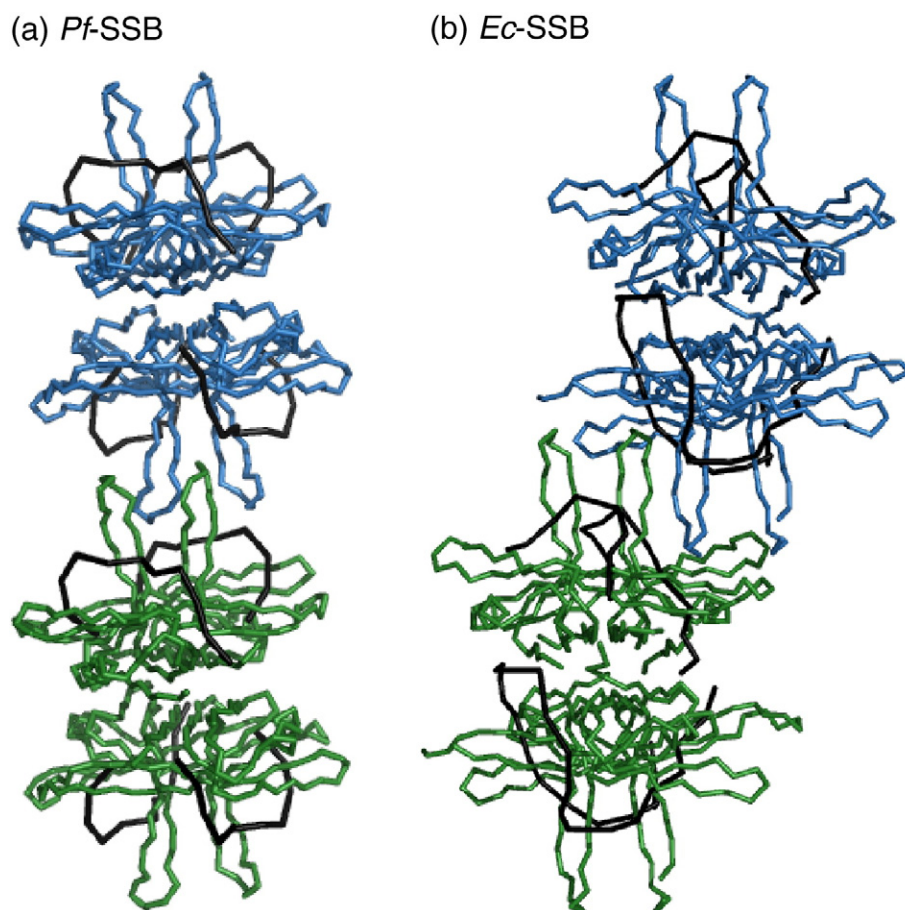


Fig. 7. Protein–protein contacts between SSB tetramers. Contacts between tetramers in neighboring unit cells in *Pf*-SSB (a) and *Ec*-SSB (b) are shown. The bound DNA in each structure is represented by the black ribbons.

more symmetric within the *Pf*-SSB complex. In the *Pf*-SSB–(dT)₃₅ structure, the DNA contacts are the same within each subunit (Figs. 3 and 4), whereas in the *Ec*-SSB–(dC)₃₅ structure, a subset of the contacts differ among the subunits.¹¹ Apart from the conformational differences observed for W40 in the *Ec*-SSB structure, it has been hypothesized that the (SSB)₃₅ binding mode is mediated by the asymmetry in the stacking interaction between the DNA and W54 situated on the β 3 extension, which is observed in only three of the four subunits.¹¹ In *Pf*-SSB, the homologous W166 residue shows stacking interactions within all four subunits of the tetramer. An *E. coli* mutant with either a W54S or a W88T mutation shows increased sensitivity to UV; however, this is not the case for a W40T substitution.⁵¹ However, biochemical studies suggest interactions between W40 and the ssDNA.⁵² A W54S mutation also results in a relative stabilization of the (SSB)₃₅ DNA binding mode in *Ec*-SSB,³⁶ and in both *Ec*-SSB and *Pf*-SSB structures, this residue forms a stacking interaction with the nucleotide. This suggests that W54 is important for promoting the fully wrapped

(SSB)₆₅ DNA binding mode. The *E. coli* *ssb-3* mutation (G15 to D) shows extreme sensitivity to UV⁵³ and is positioned close to the ssDNA in the crystal structure.¹¹ This residue is also conserved in *Pf*-SSB (G92) and is also positioned close to the DNA, suggesting a conservation of key amino acid residues between the two proteins.

The third major difference between the two structures lies in the tetramer–tetramer interface between symmetry-related molecules (Fig. 7). In all *Ec*-SSB structures solved to date, the L_{4–5} loops from neighboring tetramers pack against each other (Fig. 7b). This led to the hypothesis that this tetramer–tetramer interface might be involved in the cooperative (SSB)₃₅ DNA binding mode in *Ec*-SSB.¹¹ We do not observe such an interface in the *Pf*-SSB crystals (Fig. 7a). As shown in the accompanying paper (Antony *et al.*), *Pf*-SSB also does not appear able to form a stable (SSB)₃₅ DNA binding mode. The structure and the length of the L_{4–5} loops in the various apo- or DNA-bound crystal structures of homologous bacterial SSB proteins also appear to be similar.^{20,39,42,43} In the *Ec*-SSB structures, only the

basal half of this loop contacts the DNA. Moreover, the top parts of the L_{4-5} loops are disordered in all structures except *Ec*-SSB, where they form *inter*-tetrameric contacts that may be important for cooperative binding in the (SSB)₃₅ mode. The conserved size of the L_{4-5} loop suggests that it may be important for tetramer–tetramer interactions in other SSB homologs as well.

It is possible that some of these differences may result from the different solution conditions under which the two structures were crystallized. The *Pf*-SSB–(dT)₃₅ crystals only grew in either 0.2 M Na [Br, Cl or SO₄], whereas the *Ec*-SSB–(dC)₃₅ crystals were obtained in the absence of any added salt.¹¹ Multiple DNA binding modes have been observed with *Ec*-SSB that are dependent upon the salt concentration. The (SSB)₃₅ DNA binding mode is observed at low NaCl concentrations (<10 mM), whereas the fully wrapped (SSB)₆₅ binding mode is observed at higher NaCl concentrations (>200 mM).¹³ Our attempts to obtain crystals of *Pf*-SSB–(dT)₃₅ complexes under the low salt conditions used to obtain the *Ec*-SSB–(dC)₃₅ crystals were not successful.

A final striking difference between the *Pf*-SSB and *Ec*-SSB proteins is the sequence divergence of the unstructured C-terminus and the composition of the C-terminal amino acid end (*Pf*: MNVQEFEE *versus Ec*: DFDDDIPF). However, it is not likely that this region plays a role in determining the polarity of the bound ssDNA. In *Plasmodium*, compounds inhibiting the activity of apicoplast proteins have been used as successful antimalarial drugs.⁵⁴ Mutations in the *Ec*-SSB C-terminus render *E. coli* severely impaired for DNA repair and replication or result in lethality.⁸ Small-molecule inhibitors that inhibit the interaction of the *Ec*-SSB C-terminal tails with an array of other proteins have emerged as a new class of potential antibiotics.⁵⁵ It remains to be determined whether the sequence of the *Pf*-SSB C-terminus is important for any *Pf*-SSB interactions with any proteins important for its function in the apicoplast, although this possibility seems likely.

Materials and Methods

Buffers

Buffer H^{0.08} is 10 mM Hepes (pH 8.1), 1 mM ethylenediaminetetraacetic acid (EDTA), 0.08 M NaCl and 1 mM TCEP. Buffer H^{0.2} is 10 mM Hepes (pH 8.1), 0.1 mM Na₃EDTA, 200 mM NaCl and 5 mM 2-ME. Lysis buffer is 50 mM Tris–Cl (pH 8.3), 1 mM EDTA, 200 mM NaCl, 10% sucrose and 15 mM spermidine. Buffer T^x is 50 mM Tris–Cl (pH 8.3), 1 mM EDTA and 5% (v/v) glycerol, where “x” denotes the molar concentration of NaCl. Storage buffer is 20 mM Tris–Cl (pH 8.3), 1 mM Na₃EDTA, 500 mM NaCl, 5 mM 2-ME and 50% (v/v) glycerol.

Expression and purification of *Pf*-SSB

The *Pf*-SSB gene was amplified from genomic DNA (3D7 isolate, a kind gift from Dr. Daniel Goldberg, Washington University) using the following primers: Forward: 5′-AATTCATATGAATGAGAAATCAT-TAAAT-3′ and Reverse: 5′-AATTGGATCCTCATTCTT-CAAATCTTGG-3′, and was cloned into the pET21a vector (Novagen Inc.) using NdeI and BamHI restriction sites. The DNA encoding for the N-terminal amino acids 1–76 was omitted since it encodes the ALS.⁴ Furthermore, constructs containing the ALS signal sequence did not overexpress in *E. coli*. We refer to this version of *Pf*-SSB (residues 77–284) that lacks the ALS signal sequence as the wild-type protein.

Pf-SSB was overexpressed in BL21(DE3) cells and purified using a procedure similar to that described for *Ec*-SSB.^{48,56} All steps were carried out at 4 °C. We resuspended 30 g of cell paste in lysis buffer (150 mL) and lysed it using an Avestin cell disrupter (Avestin Inc., Canada), and we precipitated *Pf*-SSB and DNA in the clarified lysate by adding polyethyleneimine (PEI) to 0.2% (final). The protein was resuspended from the PEI pellet using 200 mL of buffer T^{0.4}. *Pf*-SSB from the PEI resuspension was precipitated by adding solid ammonium sulfate (144 g/L) (25% saturation), and the pellet containing >90% pure *Pf*-SSB was resuspended in buffer T^{0.3} (200 mL). The resuspended protein was loaded onto an ssDNA cellulose column (50 mL resin with ~3 mg/mL binding capacity) and eluted using a linear NaCl gradient (0.3–2 M) in buffer T. Fractions containing *Pf*-SSB were pooled and precipitated with 30.8% ammonium sulfate (170 g/L). The resulting precipitate was resuspended in 10 mL of storage buffer, dialyzed and stored as 0.5 mL aliquots at –20 °C. The concentration of *Pf*-SSB was determined spectrophotometrically using an extinction coefficient of $\epsilon_{280} = 9.58 \times 10^4 \text{ M}^{-1}$ (tetramer) cm^{-1} . With the use of this procedure, the typical yield of *Pf*-SSB is around 15 mg per gram of cell paste. The extinction coefficient in buffers H^{0.2} and T^{0.2} was determined by comparing the absorbance of *Pf*-SSB in buffers H^{0.2} and T^{0.2} with its absorbance in 6 M guanidinium HCl, 10 mM Tris–Cl (pH 8.1), 0.25 mM Na₃EDTA and 1 mM 2-ME at 25 °C. The extinction coefficient of the denatured *Pf*-SSB in 6 M guanidinium HCl was calculated as the sum of the extinction coefficients of the three Trp, four Tyr and three Phe in 6 M guanidinium HCl.⁵⁷ *Pf*-SSB was dialyzed extensively at 4 °C *versus* the buffers used in each experiment using a dialysis membrane with a molecular mass cutoff of 10,000 Da (Spectrum Inc., Houston, TX). *Pf*-SSB has a single exposed cysteine, and in the absence of reducing agent (5 mM 2-ME or 1 mM TCEP), it forms higher-order oligomers in solution (Fig. S1). For this reason, all experiments were performed in the presence of 1 mM TCEP.

DNA

The oligodeoxynucleotides, (dT)₃₅ and (dT)₇₀, were synthesized and purified as described previously.⁵⁸ All ssDNA concentrations were determined spectrophotometrically using the extinction coefficient $\epsilon_{260} = 8.1 \times 10^3 \text{ M}^{-1}$ (nucleotide) cm^{-1} for oligo(dT) in buffer H^{0.08}.

Analytical ultracentrifugation

Sedimentation experiments were performed using an Optima XL-A analytical ultracentrifuge equipped with an An50Ti rotor (Beckman Coulter, Fullerton, CA) at 25 °C. For sedimentation equilibrium experiments, 120 μ L of protein solution was loaded into each of the three channels of an Epon charcoal-filled six-channel centerpiece with 130 μ L of buffer in each reference channels. Protein concentration was monitored by absorbance at 280 nm at three different protein concentrations (1.04, 3.13 and 6 μ M Pf-SSB in buffer H^{0.1}). Data were collected with a spacing of 0.001 cm with an average of 10 scans per step at four rotor speeds: 9500, 11,500, 14,000 and 17,000 rpm. At each speed, sedimentation equilibrium was determined when successive scans measured over a 2-h time window were superimposable. Data sets were edited and extracted using SEDFIT^{23,24} followed by analysis by NLLS using the program SEDPHAT.⁵⁹ Apparent molecular weights were obtained by fitting the data to Eq. (1):

$$A_T = \sum_{i=1}^n \exp(\ln A_{0,i} + \sigma_i(r^2 - r_{\text{ref}}^2) / 2) + b \quad (1)$$

where A_T is the total absorbance at radial position r ; $A_{0,i}$ is the absorbance of component i at the reference radial position (r_{ref}); b is the baseline offset; $\sigma_i = [M_i(1 - \bar{v}_i \rho^0) \omega^2] / RT$ and M_i and \bar{v}_i are the molecular mass and partial specific volume of component i , respectively (calculated using SEDENTREP⁶⁰). For Pf-SSB, the \bar{v}_i value (0.7191 mL g⁻¹ at 25 °C) was calculated based on its amino acid composition (residues 77–284). The solution density ρ for buffer H^{0.1} was 1.0026 (calculated using SEDENTREP). ω is the angular velocity, R is the ideal gas constant and T is the absolute temperature. A global NLLS fit to Eq. (1) of the nine absorbance files was used to calculate the molecular weight.

Sedimentation velocity experiments (Fig. 3b) were performed using 3 μ M Pf-SSB alone or in complex with 3 μ M (dT)₇₀ (1:1 molar ratio) or 6 μ M (dT)₃₅ (1:2 molar ratio). Experiments were also performed on both (dT)₇₀ and (dT)₃₅ DNA molecules alone. We loaded 380 μ L of sample and 392 μ L of buffer into the appropriate sectors of an Epon charcoal-filled two-sector centerpiece and centrifuged them at 42,000 rpm (25 °C), and we monitored the absorbance at 280 nm. The continuous sedimentation coefficient distribution, $c(s)$, was calculated using the program SEDFIT.^{23,24}

DNA binding

Pf-SSB binding to the oligodeoxynucleotides, (dT)₇₀ or (dT)₃₅, was monitored by the quenching of the intrinsic Trp fluorescence of Pf-SSB using a PTI QM-2000 fluorometer (Photon Technologies, Inc., Lawrenceville, NJ) [λ_{ex} = 296 nm, 2-nm excitation band-pass; λ_{em} = 345 nm, 2- to 5-nm emission band-pass] with corrections applied as described previously.⁵⁷ The experiments were performed in buffer H^{0.2} at 25 °C using either 0.1 or 0.3 μ M Pf-SSB tetramer. Under these conditions, the binding affinities of Pf-SSB for (dT)₇₀ and (dT)₃₅ are too large to measure (i.e., the titrations were stoichiometric), and the intersection of the linear parts of the titration curves was used to determine the stoichiometry of DNA binding per Pf-SSB tetramer.

Crystallization and structure determination

Pf-SSB (6 mg/mL: 61 μ M tetramer) was mixed with 122 μ M (dT)₃₅ (1:2 ratio) in buffer H^{0.2} [10 mM Hepes (pH 8.1), 0.1 mM Na₃EDTA, 200 mM NaCl and 5 mM 2-ME] and dialyzed extensively *versus* buffer H^{0.2} at 4 °C. The concentration of protein after dialysis was ~3 mg/mL. Crystals were grown by vapor diffusion using the sitting-drop method in 96-well plates using a crystallization robot (Phoenix; Art Robbins Instruments, Sunnyvale, CA). The first Pf-SSB–(dT)₃₅ crystal form (bipyramidal) was observed in several commercial polyethylene glycol (PEG)-based screens [PEG/Ion HT (Hampton Research, Aliso Viejo, CA), PEGs Suite (Qiagen, Valencia, CA) and PACT premier (Molecular Dimensions, Apopka, FL)] at 20 °C after 3–4 days. The second Pf-SSB–(dT)₃₅ crystal form (long rods) was observed at 4 °C after 4–5 weeks in 0.1 M 2-[bis(2-hydroxyethyl)amino]-2-(hydroxymethyl)propane-1,3-diol propane (pH 8.5), 20% PEG 3350 and either 0.2 M sodium bromide or 0.2 M sodium sulfate. Crystals of a Pf-SSB–(dT)₃₅ complex, grown in 0.1 M 2-[bis(2-hydroxyethyl)amino]-2-(hydroxymethyl)propane-1,3-diol propane (pH 8.5), 0.15 M sodium sulfate and 24% PEG 3350 at 15 °C, were harvested into cryo-protectant solution (20% ethylene glycol, 5% PEG 3350 and 60% mother liquor) and flash frozen in liquid nitrogen. Diffraction data were collected using a 1.2-kW MM007 Rigaku generator with VHF optics and Raxis-IV++ image detector under cryo-stream with the X-stream cryo-cooling system. Data were processed with the HKL2000 program.⁶¹ Initial phases were obtained by the molecular

Table 1. Data collection and refinement statistics

Space group	C2
Unit cell parameters	
a, b, c (Å)	118.0, 82.8, 87.6
β (°)	99.57
Data collection resolution	50–2.1
R_{merge} (%) ^a	6.8 (52.9)
Completeness ^a	99.4 (97.3)
I/σ high-resolution/high resolution shell	3
Refinement resolution (Å)	30–2.1
Number of protein non-hydrogen atoms	3638
Number of DNA atoms	1022
Number of water molecules	232
Number of reflections	45,791
Number of reflection test set (5%)	2438
R (%) ^a	21.8 (28.3)
R_{free} (%) ^a	27.6 (35.4)
RMSD bonds (Å)	0.01
RMSD angles (°)	1.5
Overall B -factor, protein (Å ²)	35
Overall B -factor, DNA (Å ²)	57
Overall B -factor, solvent (Å ²)	43
Ramachandran plot (%) ^b	
Most favored regions	90.0
Allowed regions	9.0
Generously allowed ^c	1.0
Disallowed	0.0

^a Values for the highest resolution for the data collection 2.10–2.14 and for the refinement 2.10–2.15 Å are shown in parentheses.

^b Ramachandran plot parameters were calculated by program PROCHECK.⁶⁶

^c Residues in generously allowed conformation are in poorly structured loops.

replacement method using Phaser^{62,63} within the CCP4i program suite^{64,65} using the structure of the *Ec*-SSB–DNA complex¹¹ (PDB code: 1EYG).

Initial bipyramidal crystals belonging to the tetragonal space group *I*422 with unit cell parameters $a=b=83.1$ Å and $c=136.7$ Å contained one *Pf*-SSB monomer per asymmetric unit. A second crystal form was also obtained belonging to a monoclinic space group (Table 1) with one tetramer per asymmetric unit. Since the structure of the monomer in the tetragonal group was close to that of the monoclinic form, we describe the structure of the tetramer. The model building and refinement were completed using ARP/wARP,⁶⁷ Coot⁶⁸ and REFMAC.⁶⁹ Non-crystallographic averaging was not utilized during the initial model building and refinement steps. The following residues were disordered and not modeled due to poor electron density: chain A, 169–172; chain B, 121 and 171–173; chain C, 170–171; and chain D, 121–122 and 169–171. The model was refined to a resolution of 2.1 Å with $R=22.8$ and $R_{\text{free}}=27.5$ with excellent geometry (Table 1).

Accession numbers

The coordinates of the *Pf*-SSB–(dT)₃₅ complex have been deposited in the PDB with PDB ID: 3ULP.

Acknowledgements

The *P. falciparum* genomic DNA was a kind gift from Dr. Daniel Goldberg (Washington University School of Medicine). We thank Dr. Alex Kozlov and Dr. Binh Nguyen for significant technical advice and Mr. Thang Ho for synthesis and purification of the oligodeoxynucleotides. This work was supported in part by grants from the National Institutes of Health to T.M.L. (GM30498 and GM45948) and S.K. (GM073837).

Supplementary Data

Supplementary data to this article can be found online at [doi:10.1016/j.jmb.2012.04.021](https://doi.org/10.1016/j.jmb.2012.04.021)

References

1. Snow, R. W., Guerra, C. A., Noor, A. M., Myint, H. Y. & Hay, S. I. (2005). The global distribution of clinical episodes of *Plasmodium falciparum* malaria. *Nature*, **434**, 214–217.
2. Wilson, R. J., Denny, P. W., Preiser, P. R., Rangachari, K., Roberts, K., Roy, A. *et al.* (1996). Complete gene map of the plastid-like DNA of the malaria parasite *Plasmodium falciparum*. *J. Mol. Biol.* **261**, 155–172.
3. Dahl, E. L. & Rosenthal, P. J. (2008). Apicoplast translation, transcription and genome replication: targets for antimalarial antibiotics. *Trends Parasitol.* **24**, 279–284.
4. Prusty, D., Dar, A., Priya, R., Sharma, A., Dana, S., Choudhury, N. R. *et al.* (2010). Single-stranded DNA binding protein from human malarial parasite *Plasmodium falciparum* is encoded in the nucleus and targeted to the apicoplast. *Nucleic Acids Res.* **38**, 7037–7053.
5. Lohman, T. M. & Ferrari, M. E. (1994). *Escherichia coli* single-stranded DNA-binding protein: multiple DNA-binding modes and cooperativities. *Annu. Rev. Biochem.* **63**, 527–570.
6. Lohman, T. M., Bujalowski, W. & Overman, L. B. (1988). *E. coli* single strand binding protein: a new look at helix-destabilizing proteins. *Trends Biochem. Sci.* **13**, 250–255.
7. Sancar, A., Williams, K. R., Chase, J. W. & Rupp, W. D. (1981). Sequences of the *ssb* gene and protein. *Proc. Natl Acad. Sci. USA*, **78**, 4274–4278.
8. Shereda, R. D., Kozlov, A. G., Lohman, T. M., Cox, M. M. & Keck, J. L. (2008). SSB as an organizer/mobilizer of genome maintenance complexes. *Crit. Rev. Biochem. Mol. Biol.* **43**, 289–318.
9. Chrysogelos, S. & Griffith, J. (1982). *Escherichia coli* single-strand binding protein organizes single-stranded DNA in nucleosome-like units. *Proc. Natl Acad. Sci. USA*, **79**, 5803–5807.
10. Lohman, T. M. & Overman, L. B. (1985). Two binding modes in *Escherichia coli* single strand binding protein–single stranded DNA complexes. Modulation by NaCl concentration. *J. Biol. Chem.* **260**, 3594–3603.
11. Raghunathan, S., Kozlov, A. G., Lohman, T. M. & Waksman, G. (2000). Structure of the DNA binding domain of *E. coli* SSB bound to ssDNA. *Nat. Struct. Biol.* **7**, 648–652.
12. Bujalowski, W. & Lohman, T. M. (1986). *Escherichia coli* single-strand binding protein forms multiple, distinct complexes with single-stranded DNA. *Biochemistry*, **25**, 7799–7802.
13. Bujalowski, W., Overman, L. B. & Lohman, T. M. (1988). Binding mode transitions of *Escherichia coli* single strand binding protein–single-stranded DNA complexes. Cation, anion, pH, and binding density effects. *J. Biol. Chem.* **263**, 4629–4640.
14. Lohman, T. M., Overman, L. B. & Datta, S. (1986). Salt-dependent changes in the DNA binding co-operativity of *Escherichia coli* single strand binding protein. *J. Mol. Biol.* **187**, 603–615.
15. Bujalowski, W. & Lohman, T. M. (1987). Limited co-operativity in protein–nucleic acid interactions. A thermodynamic model for the interactions of *Escherichia coli* single strand binding protein with single-stranded nucleic acids in the “beaded”, (SSB)₆₅ mode. *J. Mol. Biol.* **195**, 897–907.
16. Griffith, J. D., Harris, L. D. & Register, J., III (1984). Visualization of SSB–ssDNA complexes active in the assembly of stable RecA–DNA filaments. *Cold Spring Harbor Symp. Quant. Biol.* **49**, 553–559.
17. Roy, R., Kozlov, A. G., Lohman, T. M. & Ha, T. (2007). Dynamic structural rearrangements between DNA binding modes of *E. coli* SSB protein. *J. Mol. Biol.* **369**, 1244–1257.
18. Roy, R., Kozlov, A. G., Lohman, T. M. & Ha, T. (2009). SSB protein diffusion on single-stranded DNA stimulates RecA filament formation. *Nature*, **461**, 1092–1097.

19. Shamoo, Y., Friedman, A. M., Parsons, M. R., Konigsberg, W. H. & Steitz, T. A. (1995). Crystal structure of a replication fork single-stranded DNA binding protein (T4 gp32) complexed to DNA. *Nature*, **376**, 362–366.
20. Bernstein, D. A., Eggington, J. M., Killoran, M. P., Misić, A. M., Cox, M. M. & Keck, J. L. (2004). Crystal structure of the *Deinococcus radiodurans* single-stranded DNA-binding protein suggests a mechanism for coping with DNA damage. *Proc. Natl Acad. Sci. USA*, **101**, 8575–8580.
21. Wold, M. S. (1997). Replication protein A: a heterotrimeric, single-stranded DNA-binding protein required for eukaryotic DNA metabolism. *Annu. Rev. Biochem.* **66**, 61–92.
22. Norais, C. A., Chittani-Pattu, S., Wood, E. A., Inman, R. B. & Cox, M. M. (2009). DdrB protein, an alternative *Deinococcus radiodurans* SSB induced by ionizing radiation. *J. Biol. Chem.* **284**, 21402–21411.
23. Dam, J. & Schuck, P. (2004). Calculating sedimentation coefficient distributions by direct modeling of sedimentation velocity concentration profiles. *Methods Enzymol.* **384**, 185–212.
24. Schuck, P. (1998). Sedimentation analysis of noninteracting and self-associating solutes using numerical solutions to the Lamm equation. *Biophys. J.* **75**, 1503–1512.
25. Krauss, G., Sindermann, H., Schomburg, U. & Maass, G. (1981). *Escherichia coli* single-strand deoxyribonucleic acid binding protein: stability, specificity, and kinetics of complexes with oligonucleotides and deoxyribonucleic acid. *Biochemistry*, **20**, 5346–5352.
26. Bujalowski, W. & Lohman, T. M. (1989). Negative cooperativity in *Escherichia coli* single strand binding protein–oligonucleotide interactions. II. Salt, temperature and oligonucleotide length effects. *J. Mol. Biol.* **207**, 269–288.
27. Lohman, T. M. & Bujalowski, W. (1988). Negative cooperativity within individual tetramers of *Escherichia coli* single strand binding protein is responsible for the transition between the (SSB)₃₅ and (SSB)₅₆ DNA binding modes. *Biochemistry*, **27**, 2260–2265.
28. Bujalowski, W. & Lohman, T. M. (1989). Negative cooperativity in *Escherichia coli* single strand binding protein–oligonucleotide interactions. I. Evidence and a quantitative model. *J. Mol. Biol.* **207**, 249–268.
29. Gallagher, J. R., Matthews, K. A. & Prigge, S. T. (2011). *Plasmodium falciparum* apicoplast transit peptides are unstructured *in vitro* and during apicoplast import. *Traffic*, **12**, 1124–1138.
30. McFadden, G. I. (1999). Plastids and protein targeting. *J. Eukaryotic Microbiol.* **46**, 339–346.
31. Ng, J. D. & McPherson, A. (1989). Preliminary crystallographic analysis of a proteolytically modified form of *E. coli* single stranded DNA binding protein. *J. Biomol. Struct. Dyn.* **6**, 1071–1076.
32. Thorn, J. M., Carr, P. D., Chase, J. W., Dixon, N. E. & Ollis, D. L. (1994). Crystallization and low temperature diffraction studies of the DNA binding domain of the single-stranded DNA binding protein from *Escherichia coli*. *J. Mol. Biol.* **240**, 396–399.
33. Ollis, D., Brick, P., Abdel-Meguid, S. S., Murthy, K., Chase, J. W. & Steitz, T. A. (1983). Crystals of *Escherichia coli* single-strand DNA-binding protein show that the tetramer has D_2 symmetry. *J. Mol. Biol.* **170**, 797–800.
34. Murzin, A. G. (1993). OB(oligonucleotide/oligosaccharide binding)-fold: common structural and functional solution for non-homologous sequences. *EMBO J.* **12**, 861–867.
35. Curth, U., Bayer, I., Greipel, J., Mayer, F., Urbanke, C. & Maass, G. (1991). Amino acid 55 plays a central role in tetramerization and function of *Escherichia coli* single-stranded DNA binding protein. *Eur. J. Biochem.* **196**, 87–93.
36. Curth, U., Greipel, J., Urbanke, C. & Maass, G. (1993). Multiple binding modes of the single-stranded DNA binding protein from *Escherichia coli* as detected by tryptophan fluorescence and site-directed mutagenesis. *Biochemistry*, **32**, 2585–2591.
37. Ferrari, M. E., Fang, J. & Lohman, T. M. (1997). A mutation in *E. coli* SSB protein (W54S) alters intratetramer negative cooperativity and inter-tetramer positive cooperativity for single-stranded DNA binding. *Biophys. Chem.* **64**, 235–251.
38. Carlini, L. E. & Porter, R. D. (1997). Analysis of ssb mutations *in vivo* implicates SSB protein in two distinct pathways of SOS induction and in recombinational DNA repair. *Mol. Microbiol.* **24**, 129–139.
39. Chan, K. W., Lee, Y. J., Wang, C. H., Huang, H. & Sun, Y. J. (2009). Single-stranded DNA-binding protein complex from *Helicobacter pylori* suggests an ssDNA-binding surface. *J. Mol. Biol.* **388**, 508–519.
40. Raghunathan, S., Ricard, C. S., Lohman, T. M. & Waksman, G. (1997). Crystal structure of the homotetrameric DNA binding domain of *Escherichia coli* single-stranded DNA-binding protein determined by multiwavelength X-ray diffraction on the selenomethionyl protein at 2.9-Å resolution. *Proc. Natl Acad. Sci. USA*, **94**, 6652–6657.
41. Fedorov, R., Witte, G., Urbanke, C., Manstein, D. J. & Curth, U. (2006). 3D structure of *Thermus aquaticus* single-stranded DNA-binding protein gives insight into the functioning of SSB proteins. *Nucleic Acids Res.* **34**, 6708–6717.
42. Kaushal, P. S., Singh, P., Sharma, A., Muniyappa, K. & Vijayan, M. (2010). X-ray and molecular-dynamics studies on *Mycobacterium leprae* single-stranded DNA-binding protein and comparison with other eubacterial SSB structures. *Acta Crystallogr., Sect. D: Biol. Crystallogr.* **66**, 1048–1058.
43. Saikrishnan, K., Jeyakanthan, J., Venkatesh, J., Acharya, N., Sekar, K., Varshney, U. & Vijayan, M. (2003). Structure of *Mycobacterium tuberculosis* single-stranded DNA-binding protein. Variability in quaternary structure and its implications. *J. Mol. Biol.* **331**, 385–393.
44. Yang, C., Curth, U., Urbanke, C. & Kang, C. (1997). Crystal structure of human mitochondrial single-stranded DNA binding protein at 2.4 Å resolution. *Nat. Struct. Biol.* **4**, 153–157.
45. Yadav, T., Carrasco, B., Myers, A. R., George, N. P., Keck, J. L. & Alonso, J. C. (2012). Genetic recombination in *Bacillus subtilis*: a division of labor between two single-strand DNA-binding proteins. *Nucleic Acids Res.*, <http://dx.doi.org/10.1093/nar/gks173>.
46. Bujalowski, W. & Lohman, T. M. (1991). Monomers of the *Escherichia coli* SSB-1 mutant protein bind single-stranded DNA. *J. Mol. Biol.* **217**, 63–74.

47. Williams, K. R., Murphy, J. B. & Chase, J. W. (1984). Characterization of the structural and functional defect in the *Escherichia coli* single-stranded DNA binding protein encoded by the *ssb-1* mutant gene. Expression of the *ssb-1* gene under λ P_L regulation. *J. Biol. Chem.* **259**, 11804–11811.
48. Bujalowski, W. & Lohman, T. M. (1991). Monomer–tetramer equilibrium of the *Escherichia coli* *ssb-1* mutant single strand binding protein. *J. Biol. Chem.* **266**, 1616–1626.
49. Meyer, R. R., Glassberg, J., Scott, J. V. & Kornberg, A. (1980). A temperature-sensitive single-stranded DNA-binding protein from *Escherichia coli*. *J. Biol. Chem.* **255**, 2897–2901.
50. Meyer, R. R., Glassberg, J. & Kornberg, A. (1979). An *Escherichia coli* mutant defective in single-strand binding protein is defective in DNA replication. *Proc. Natl Acad. Sci. USA*, **76**, 1702–1705.
51. Carlini, L. E., Porter, R. D., Curth, U. & Urbanke, C. (1993). Viability and preliminary *in vivo* characterization of site-directed mutants of *Escherichia coli* single-stranded DNA-binding protein. *Mol. Microbiol.* **10**, 1067–1075.
52. Khamis, M. I., Casas-Finet, J. R., Maki, A. H., Murphy, J. B. & Chase, J. W. (1987). Investigation of the role of individual tryptophan residues in the binding of *Escherichia coli* single-stranded DNA binding protein to single-stranded polynucleotides. A study by optical detection of magnetic resonance and site-selected mutagenesis. *J. Biol. Chem.* **262**, 10938–10945.
53. Meyer, R. R. & Laine, P. S. (1990). The single-stranded DNA-binding protein of *Escherichia coli*. *Microbiol. Rev.* **54**, 342–380.
54. McFadden, G. I. & Roos, D. S. (1999). Apicomplexan plastids as drug targets. *Trends Microbiol.* **7**, 328–333.
55. Lu, D., Bernstein, D. A., Satyshur, K. A. & Keck, J. L. (2010). Small-molecule tools for dissecting the roles of SSB/protein interactions in genome maintenance. *Proc. Natl Acad. Sci. USA*, **107**, 633–638.
56. Lohman, T. M., Green, J. M. & Beyer, R. S. (1986). Large-scale overproduction and rapid purification of the *Escherichia coli* *ssb* gene product. Expression of the *ssb* gene under λ P_L control. *Biochemistry*, **25**, 21–25.
57. Lohman, T. M. & Mascotti, D. P. (1992). Nonspecific ligand–DNA equilibrium binding parameters determined by fluorescence methods. *Methods Enzymol.* **212**, 424–458.
58. Ferrari, M. E., Bujalowski, W. & Lohman, T. M. (1994). Co-operative binding of *Escherichia coli* SSB tetramers to single-stranded DNA in the (SSB)₃₅ binding mode. *J. Mol. Biol.* **236**, 106–123.
59. Vistica, J., Dam, J., Balbo, A., Yikilmaz, E., Mariuzza, R. A., Rouault, T. A. & Schuck, P. (2004). Sedimentation equilibrium analysis of protein interactions with global implicit mass conservation constraints and systematic noise decomposition. *Anal. Biochem.* **326**, 234–256.
60. Laue, T. M., Shah, B. D., Rldgeway, T. M. & Pelletier, S. L. (1992). pp. 1, Royal Society of Cambridge, Cambridge, UK.
61. Otwinowski, Z. & Minor, W. (1997). Processing of X-ray diffraction data collected in oscillation mode. *Macromol. Crystallogr., Pt. A*, **276**, 307–326.
62. McCoy, A. J., Grosse-Kunstleve, R. W., Adams, P. D., Winn, M. D., Storoni, L. C. & Read, R. J. (2007). Phaser crystallographic software. *J. Appl. Crystallogr.* **40**, 658–674.
63. McCoy, A. J. (2007). Solving structures of protein complexes by molecular replacement with Phaser. *Acta Crystallogr., Sect. D: Biol. Crystallogr.* **63**, 32–41.
64. Potterton, E., Briggs, P., Turkenburg, M. & Dodson, E. (2003). A graphical user interface to the CCP4 program suite. *Acta Crystallogr., Sect. D: Biol. Crystallogr.* **59**, 1131–1137.
65. Winn, M. D., Ballard, C. C., Cowtan, K. D., Dodson, E. J., Emsley, P., Evans, P. R. *et al.* (2011). Overview of the CCP4 suite and current developments. *Acta Crystallogr., Sect. D: Biol. Crystallogr.* **67**, 235–242.
66. Laskowski, R. A., Moss, D. S. & Thornton, J. M. (1993). Main-chain bond lengths and bond angles in protein structures. *J. Mol. Biol.* **231**, 1049–1067.
67. Langer, G., Cohen, S. X., Lamzin, V. S. & Perrakis, A. (2008). Automated macromolecular model building for X-ray crystallography using ARP/wARP version 7. *Nat. Protoc.* **3**, 1171–1179.
68. Emsley, P., Lohkamp, B., Scott, W. G. & Cowtan, K. (2010). Features and development of Coot. *Acta Crystallogr., Sect. D: Biol. Crystallogr.* **66**, 486–501.
69. Winn, M. D., Murshudov, G. N. & Papiz, M. Z. (2003). Macromolecular TLS refinement in REFMAC at moderate resolutions. *Methods Enzymol.* **374**, 300–321.